The accuracy of local rib bone geometry measurement using full body CT images

Sven A. Holcombe[1], Yun-Seok Kang[2], Stewart C. Wang[1], Amanda M. Agnew[2]

[1] University of Michigan, International Center for Automotive Medicine
[1] The Ohio State University, Injury Biomechanics Research Center

Abstract The ribs play a key structural role in the chest during dynamic loading, and future safety advancements will increasingly rely on the biofidelity of Human Body Models (HBMs). Rib geometry in HBMs is typically obtained via global imaging from CT, however for thin cortices such as those in ribs, traditional histogram-based segmentation is known to produce unacceptably high error. Here we test the accuracy of a new cortical bone mapping (CBM) algorithm in resolving these local geometries from globally obtained full-body CT scans, as well as from higher resolution scans of isolated ribs. Results from 11 cadaveric subjects' scanned ribs are compared to ground truth histology obtained from specific rib sections.

The CBM methodology resolved the local thickness of cortical bone from isolated rib scans to within 0.01±0.14mm (mean±SD) error, and from full body scans to -0.04±0.20mm error. Average positional error in the placement of the rib's periosteal border was -0.01±0.13mm from full body scans using CBM, compared to 0.81±0.42mm for histogram-based thresholding of those same scans. Consequently, important mechanical properties are resolved to much higher accuracy using CBM, with total rib cross sectional area error reduced from 39±12% under traditional thresholding to under 5±2% when obtained using CBM.

This study has shown that – given appropriate extraction methodologies – local geometric properties of rib bones can be obtained from full-body CT imaging of human subjects. Results from this study open the door for subject-specific rib cortical bone thickness maps to be obtained for HBM validation and improvement.

Keywords Rib, CT, Cortical bone, CBM, thickness, geometry, cross-section.

I. INTRODUCTION

The ribs play a key structural role in the chest during dynamic loading and protect multiple vital organs in a range of motor vehicle crash (MVCs) scenarios. Many vehicle safety systems are designed to engage the chest and the ribs, and improvements in occupant protection via these systems have gone hand in hand with advancements in understanding human rib biomechanics. Nevertheless, while injuries to other body regions are being reduced, thoracic injuries and their associated high rates of morbidity and mortality, remain constant, and particularly problematic for the elderly [1-3].

The next generation of vehicles and advanced safety systems will increasingly rely on computer simulation to explore potentially injurious conditions, and this comes with a greater reliance on the accuracy and biofidelity of human body models (HBMs). In general, rib geometry in current HBMs incorporates (1) a global or overall rib shape, (2) a cross-sectional cortex shape that can vary along the rib, and (3) a cortex thickness that can vary across the whole rib. These properties are important predictors of a rib's response to loading [4-7], and the primary source for rib bone geometry in HBMs is Computed Tomography (CT) medical imaging.

Global rib geometry is well visualized through CT imaging, and medical CT images have been used to quantify changes in overall rib and rib cage shape across different populations [8-13]. However, with the field of view in live subject CT imaging covering the full span of the chest, there are relatively few pixels available to visualize smaller structures such as rib cross sections or bone cortices. Consequently, the thickness and cross-sectional shape of rib cortical bone is less well understood.

S. A. Holcombe, Ph.D. (svenho@umich.edu), is a research scientist at the University of Michigan in the International Center for Automotive Medicine (ICAM). S. C. Wang, Ph.D., M.D., is a University of Michigan Professor of Surgery and director of ICAM. A. M. Agnew, Ph.D. is Director of the Skeletal Biology Research Laboratory and Associate Professor Emeritus at Ohio State University. Yun Seok Kang, PhD is an Assistant Professor at the School of Health & Rehabilitation Sciences, Ohio State University.

Traditional techniques for obtaining bone geometry from CT are based upon histogram-based thresholding to identify bone pixels reaching a certain image intensity. For thin structures such as rib cortices – which at 0.1 to 3.0 mm in width can be smaller in size than even the image pixels themselves – simple thresholding is unable to resolve true bone thickness [14] and can lead to unacceptably high errors in key rib geometric properties [15].

More recently, a Cortical Bone Mapping (CBM) technique has been developed that uses local optimizations to fit a model of the expected image pixels near transitions across bone cortices to the underlying CT pixels themselves [16,17]. This technique has been adapted to 2D CT images of harvested sections of rib bones where it has shown the ability to resolve bone structures to sub-pixel accuracy [18].

This study further explores the utility of CBM by assessing local accuracy in rib geometry using 3D CT image volumes – taken both from full-body CT scans at resolutions similar to clinical settings and from isolated whole rib CT scans at a higher resolution. Ground truth measurements are obtained from ultra-high resolution microscopy of specific sites taken from those same physical ribs. Geometric results obtained through CBM are also compared to traditional thresholding methods, highlighting the gains in accuracy that can be obtained using CBM. Computational HBMs rely on rib geometry built from full-body image volumes yet the veracity of small yet mechanically important structures within that geometry remain untested. Therefore, the specific objective of this study was to evaluate the precision and accuracy of CBM compared to traditional methods, and to test whether CBM when applied to full body clinical scans could supply rib cross-sectional and bone thickness measurements relevant to HBMs.

II. METHODS

Study population and image sources

Images in multiple modalities were ethically obtained from 11 anatomical donors in Ohio, USA. The 9 male subjects and 2 female subjects ranged from 54-83 years of age (mean 66), and were free of gross pathological conditions that may affect the ribs. Soon after death, subjects underwent full body clinical CT scanning (fbCT) in a supine position. The 6th ribs on one side from each subject were then excised, and further CT scans were obtained at a higher resolution using these isolated ribs (rbCT). After experimental bending tests causing fracture, transverse cross-sections were taken immediately adjacent to each fracture site while ensuring no disruption to the bone cortex. Two of the 11 ribs had two separate fracture sites for a total of 13 transverse cross-sections. Slides were then prepared according to undecalcified hard tissue histology standards (see [4]) to obtain histological images at extremely high resolution. The histology images can be considered physical ground truth as they are generated directly from the source sample and without reconstruction. The rbCT and fbCT images are reconstructed at resolutions higher than, and similar to, those typically seen in clinical settings. The full resolution specifications are given in table 1, and Fig. 1 gives a visual comparison of the different modalities from three exemplar subjects. In Fig. 1, each CT-based image comes from reslicing the original volume along an angled plane located at a spatially equivalent site to the physical histology cross-sections.

TABLE 1
IMAGE AND IMAGE VOLUME CAPTURE SPECIFICATIONS

	Histology	**Isolated Rib CT**	**Full Body CT**
Description and field of view (FOV)	Cross-sectional microscopy of a single slice through rib	Scan FOV covers whole harvested rib	Scan FOV covers whole body
Acquisition spec.	Olympus BX61VS	Phillips Vereos digital PET/CT	Siemens Somatom Plus 4 CT
In-plane px/voxel size	0.69 microns	0.15 mm	0.98-1.52 mm
Slice spacing	~80 microns	0.67 mm	0.40-0.63 mm

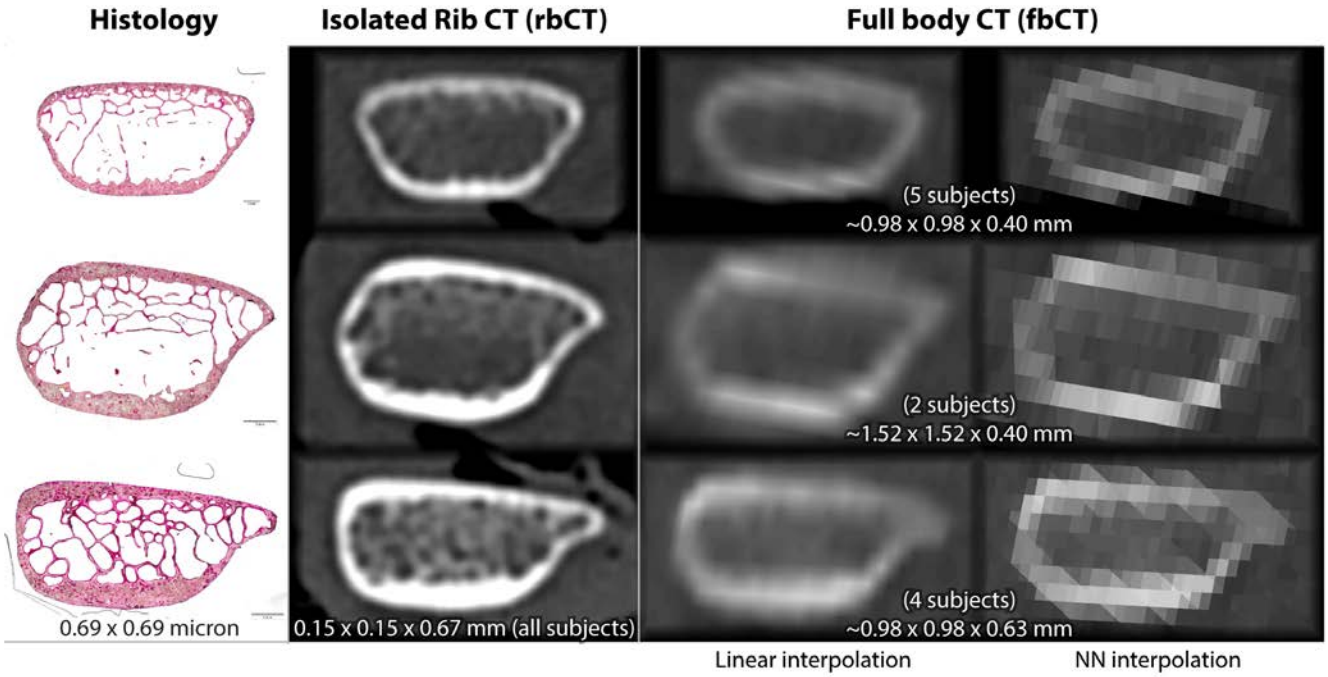

Fig. 1. Image comparison between histology images and spatially equivalent CT image reconstructed via linearly interpolated virtual cuts through the 3D image space. For demonstration, the fbCT cuts are also shown using nearest-neighbor interpolation (far right) in order to highlight the underlying voxel size and structure. For the much higher resolution rbCT image volumes, cuts using nearest neighbor vs. linear interpolation are visually indistinguishable when displayed within this manuscript.

The periosteal and endosteal borders of the cortical shell were extracted from all image modalities (see below for details). For histology images, the borders were only available at the specific cross-sectional sites at which histology was obtained. For each CT modality a full periosteal and endosteal surface was calculated using a CBM algorithm implemented in MATLAB (see below for details). The accuracy of the rbCT and fbCT surfaces were assessed against gold standard histology borders in locations where histology was available. In all cases, accuracy (mean error) and precision (SD error) was calculated for local cortical bone thickness measurements (Ct.Th), as well as whole cross-sectional properties (rib cortical bone area Ct.Ar, endosteal area Es.Ar, and area intertial moments).

CT image processing

The general application of the Cortical Bone Mapping (CBM) algorithm begins with a known but approximate position in 3D image space of a bone's periosteal border along with a direction vector pointing through that bone's cortex, and then CBM is used to refine that initial approximate position to predict both the true periosteal location and the true endosteal border location in that vicinity.

Therefore, each of the 22 ribs (11 subjects, both rbCT and fbCT) underwent initial segmentation using MIMICS (v19, Materialise) to produce an approximate 3D periosteal rib surface. This segmentation process consisted of (1) thresholding at a standard (226 HU) bone intensity; (2) morphological closing of 1 voxel; (3) cavity filling in each image plane; (4) manual editing to close remaining holes within the periosteum; (5) 3D surface (STL) generation with one iteration of mesh smoothing with a 0.3 mm smoothing kernel. All subsequent steps were performed using custom MATLAB (2019a, The Mathworks) algorithms.

The initial periosteal surface was discretized along its central axis into 301 successive and equally spaced cross-sections, with each section further discretized to 80 locations around its circumference. The pleural and cutaneous rib aspects were determined for rbCT surfaces via the secondary inertial axis of individual cross-sections, and these were projected onto the fbCT surfaces for spatial consistency between the gridded surfaces from each modality.

The CBM algorithm was then applied to every 301-by-80 surface grid location by sampling the CT image volume in a direction normal to the 3D surface at that location to generate a series of 1D image signals. By using non-linear optimization, the CBM estimates the step-like signal that best fits each of the more gradually-changing CT

image samples obtained across the ribs cortex. The transitions in the fitted stepped signal mark the new estimations of the true periosteal and endosteal cortex borders. The CBM parameter representing the expected cortical bone density was assigned for rbCT images as the 99th percentile in peak image intensity values taken across the full rib's surface. The CBM optimization routine included weighting to more aggressively penalize model fitting errors located near the initial periosteal surface. After the first CBM iteration was performed, the CBM routine was repeated using the newly predicted periosteal border location so as to ensure that this weighted location was more closely aligned with the true periosteum than in the initial approximated surface.

To extend the CBM methodology for 2D rib sections used in [18] to the 3D data used here and to reduce high-frequency noise in the final periosteal and endostea border surfaces, an additional error-based local smoothing step was applied to each. Specifically, a 0.3 mm Gaussian-shaped smoothing kernel was used that was further scaled by the inverse of the CBM model fitting error at those same locations. Finally, as each of the 301 cross-sections along the rib were inspected to discard data from any signals which did not pass through a single isolated cortical wall as described for 2D cross-sections in [18].

Histology image processing for ground truth geometry

Periosteal and endosteal cortical borders were semi-manually identified on each histology image using ImageJ software (NIH) by an experienced bone histologist (AA)[19]. Spatial registration was achieved between the histology images and the CT volumes by choosing the cross-sectional location that gave minimal rigid registration error between the periosteal borders from histology and successive CT cross-sectional cuts of the same rib.

Accuracy assessment and other comparisons

Two types of measurements were taken from the borders predicted by the CBM methodology from both CT modalities. Firstly, point-wise local measures of cortical bone thickness (Ct.Th), and secondly, measures of area and inertial moment properties taken from a full cross-section through the rib. Specifically, the total area within the predicted periosteal border (Tt.Ar), the area within the endosteal border (Es.Ar), the cortical bone area between the endosteal and periosteal borders (Ct.Ar), and the area moments of inertia (Ix, Iy) of this cortical bone shell were used. These measurements were all tested against ground truth from histology in terms of their measurement accuracy (mean error across all samples) and precision (SD error). Finally, a local geometric error was calculated simply as the linear distance between the predicted position of the periosteal (or endosteal) border when using rbCT or fbCT against the true position of that border as seen on histology.

To assess the benefit gained by the use of CBM over traditional methods, the initial smooth surface that was segmented manually from fbCT using histogram-based thresholding was used to take additional measurements of (Tt.Ar) and the local geometric error in the periosteal border position.

Finally, to explore the applicability of the CBM algorithm to ribs *in vivo* vs. *ex vivo* – particularly the effect of having tissue of various densities adjacent to whole ribs – the whole rib surface Ct.Th results obtained from full body (fbCT) scans were compared to those from isolated rib (rbCT) scans.

III. RESULTS

The CBM method was successfully applied across the bone surfaces in all isolated rib scans (rbCT) and full body scans (fbCT). Exemplar cross-sectional snapshots at 10 percentile intervals along three subjects ribs are displayed in Fig. 2. These highlight the variation in rib cross-sectional shape along its length, the differences in image resolution between CT modalities, and, notably, the overall similarities in predicted periosteal and endosteal borders between the two modalities. Equivalent images from all subjects are included as supplemental material.

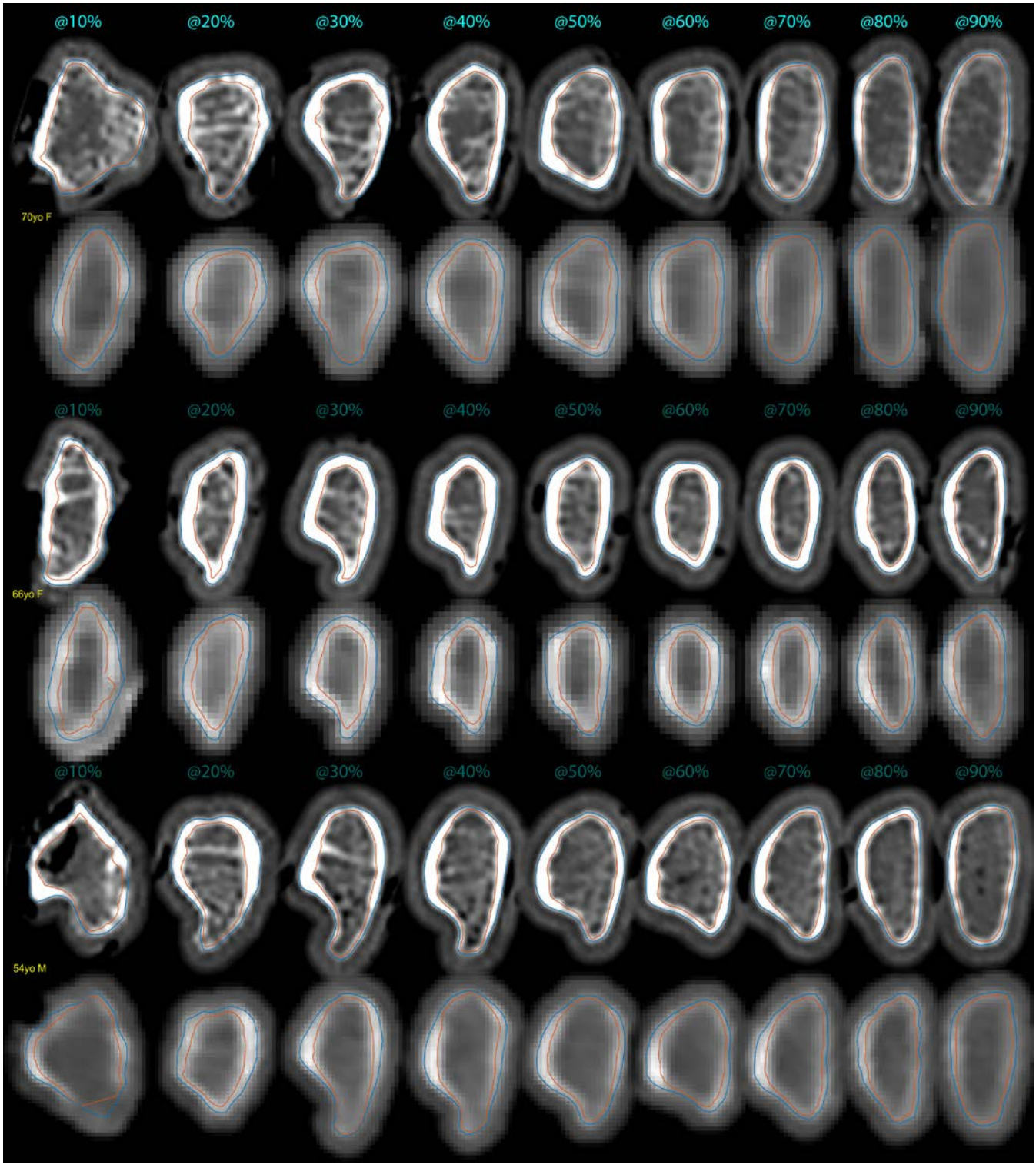

Fig. 2.Cross-sectional comparison pairs of extracted periosteal and endosteal borders from three subjects' rbCT (pair above) and fbCT (pair below) scans along the length of ribs (left to right).

Fig. 3 highlights the specific cross-sectional positions along each rib (one or two per rib) that match histology images for ground truth comparison. Here, the extracted cortical shells between the periosteal and endosteal borders that were obtained using only the rbCT or fbCT data sources are overlaid onto each equivalent histology section image. Comparisons of the cross-sectional geometric measures (areas, inertial moments) for these whole cross sections as compared to the underlying histology image are provided as scatter plots in Fig. 4, and the accuracy (mean measurement error) and precision (SD error) of the rbCT and fbCT scans in predicting these overall geometric measures are listed in Table 2.

Taking into account each individually predicted periostea/endosteal border (i.e., 80 sites around each cross section), Fig. 5 shows a scatter plot of local thickness predictions from both CT modalities against ground truth histology. Overall error distributions are also shown for local thickness measurements (Ct.Th) as well as for the final predicted positions of the endosteal/periosteal borders, with accuracy and precision of each of these local measurements listed in Table 2.

The higher resolution rbCT images were more precise (lower error SD) than fbCT images for all measurements of overall cross-sectional geometry and of local thickness and cortex position. The rbCT images were also more accurate in terms of local Ct.Th and cortical bone cross-sectional area (Ct.Ar). However, the rbCT images predicted periosteal borders marginally outside the ground truth position (by 0.11 ± 0.07 mm), meaning that total and endosteal cross-sectional area (Tt.Ar, Es.Ar) measurements were overestimated on average by 5% compared to fbCT, which had less than 2% average error. Linear correlation coefficients (R2) with histology for Ct.Ar were 0.94 (rbCT) and 0.75 (fbCT) and were above 0.99 for Tt.Ar and Es.Ar (rbCT) and 0.97 (fbCT).

Finally, when comparing the slight resolution differences between fbCT scans of all subjects it was found that the fbCT configuration with highest resolution (0.98 x 0.98 x 0.4 mm pixels) was more accurate (Ct.Th errors of 0.01 ± 0.16 mm compared to histology) than those fbCT with other resolutions (Ct.Th errors of -0.07 ± 0.21 mm, $p < 0.0001$).

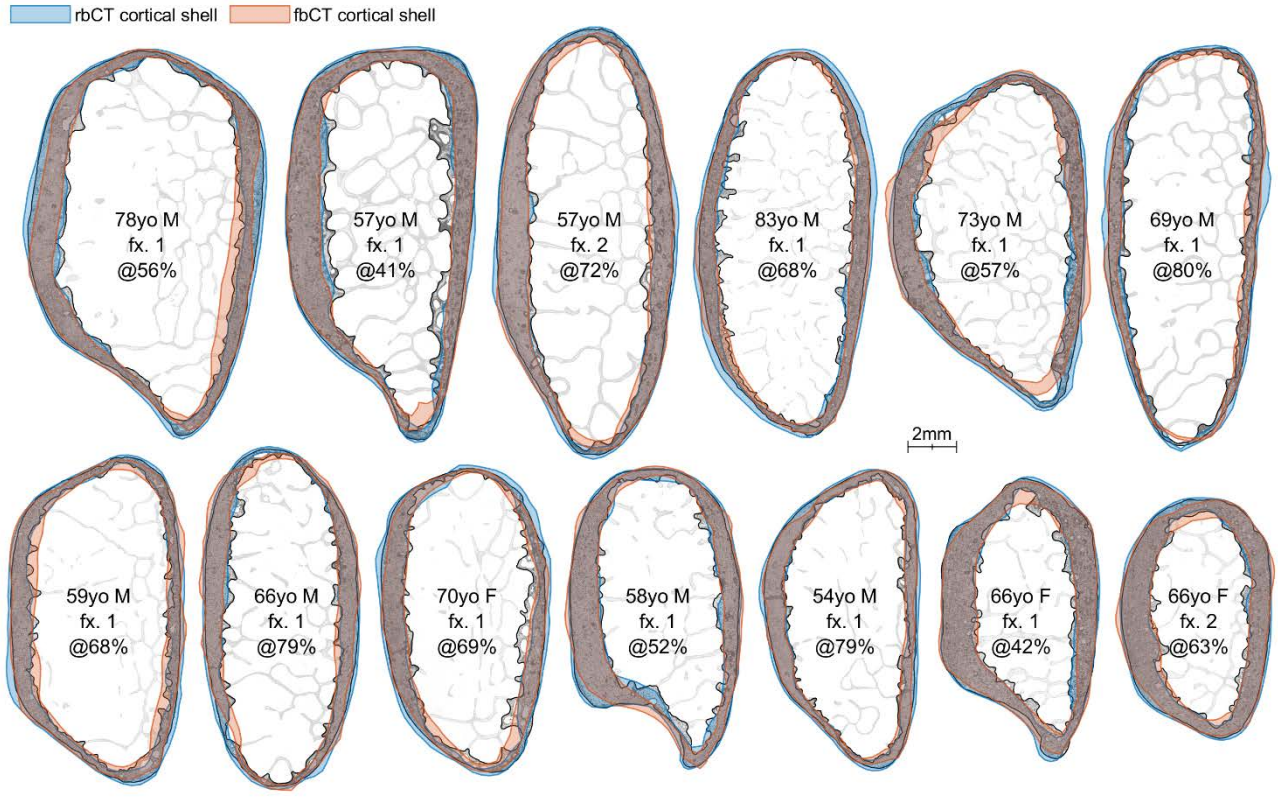

Fig. 3. Extracted cortical shells obtained using rbCT and fbCT, and superimposed onto ground truth histology images. Both modalities show strong spatial agreement to true cortical shells, even in thin cortex regions.

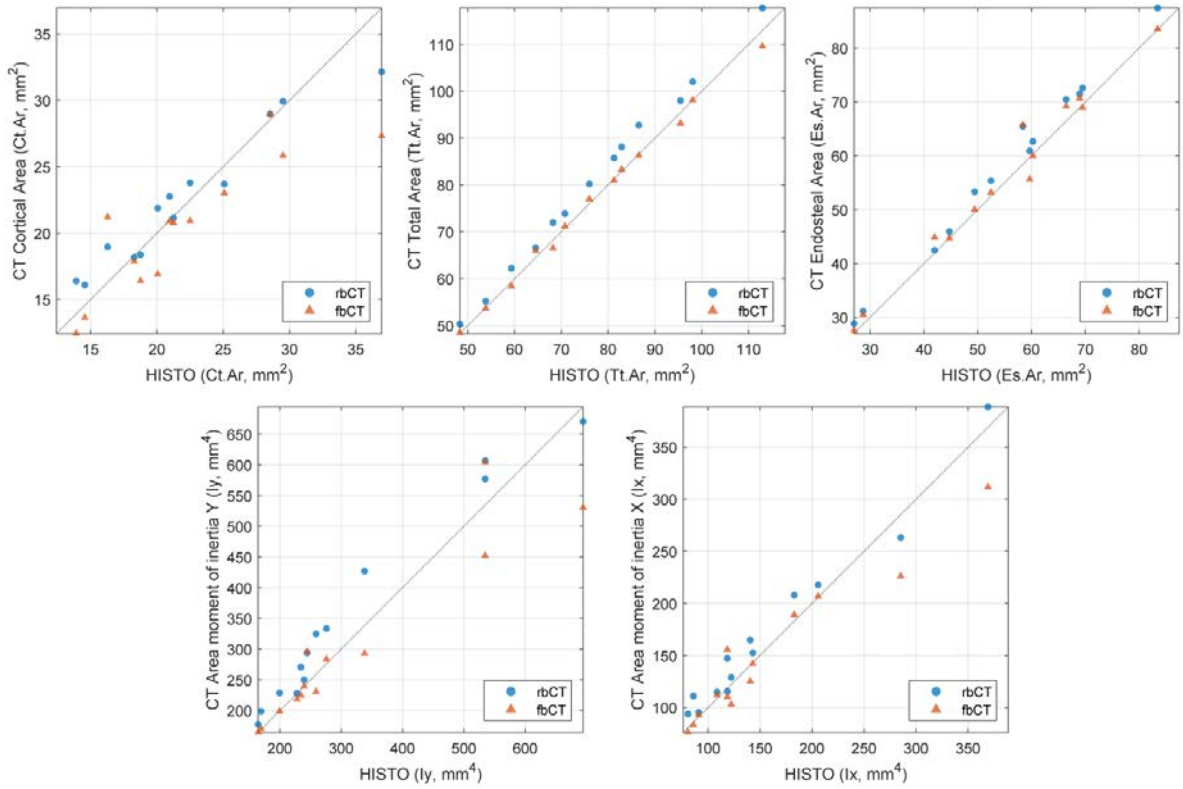

Fig. 4. Comparisons of cross-sectional geometric properties (areas, moments of inertia) between ground truth histology measurements and rbCT and fbCT predictions.

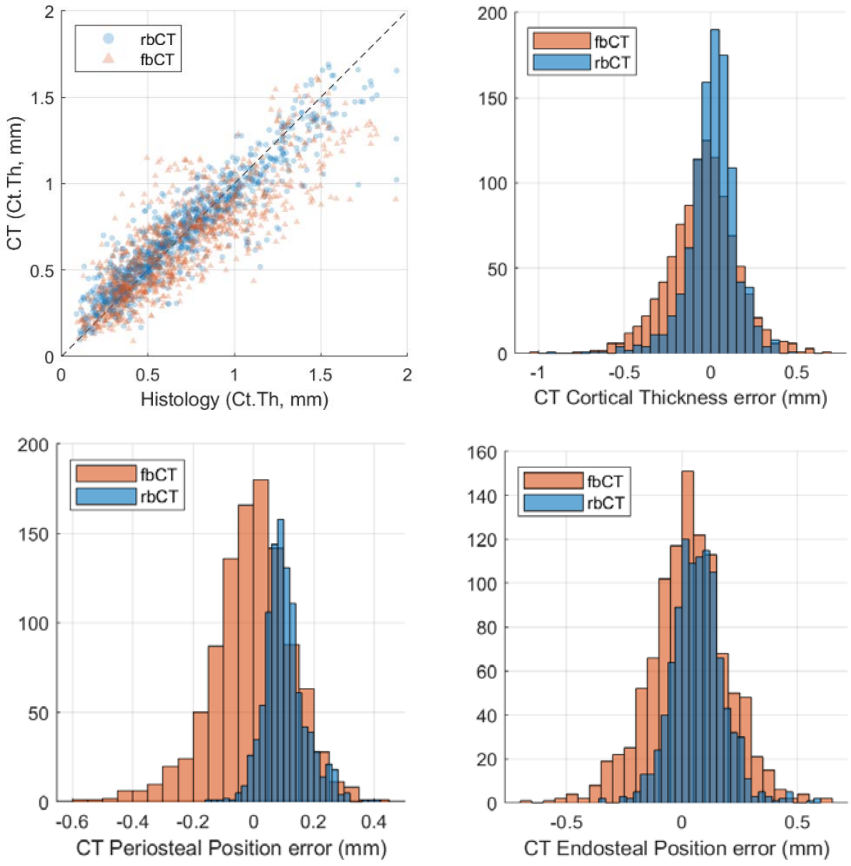

Fig. 5. Discrete rbCT and fbCT cortical bone thickness measurements compared to spatially equivalent gold standard values from histology. Positive endosteal/periosteal position errors indicate bias towards the outside of the rib, negative errors indicate bias towards the inside of the rib.

TABLE 2
ACCURACY AND PRECISION OF CORTEX GEOMETRY FROM RBCT AND FBCT WHEN COMPARED TO GROUND TRUTH HISTOLOGY

			Histology	**Isolated Rib (rbCT)**		**Full Body (fbCT)**	
Measure	Abbrev.	Units	Mean ± SD	Error	% Error	Error	% Error
Cortical bone shell area	*Ct.Ar*	mm^2	22.1 ± 5.0	0.4 ± 1.9	4 ± 8	-1.6 ± 3.1	-6 ± 13
Total periosteal area	*Tt.Ar*	mm^2	76.8 ± 18.8	3.6 ± 1.3	5 ± 1	-0.4 ± 1.3	-0.4 ± 2
Total endosteal area	*Es.Ar*	mm^2	54.7 ± 16.4	2.9 ± 1.6	5 ± 3	1.0 ± 2.5	2 ± 4
Shell inertial moments	*Ix*	mm^4	157.9 ± 18.2	11.5 ± 12.4	10 ± 10	-9.1 ± 24.6	-3 ± 12
	Iy	mm^4	316.6 ± 159.0	36.2 ± 30.1	13 ± 9	-16.2 ± 56.0	-3 ± 11
Local cortical thickness	*Ct.Th*	mm	2.545	0.01 ± 0.14	9 ± 31	-0.04 ± 0.20	2 ± 35
Local periosteal position		mm		0.10 ± 0.06		-0.01 ± 0.13	
Local endosteal position		mm		0.07 ± 0.11		0.03 ± 0.17	

When considering the initial periosteal border obtained using histogram-based thresholding (i.e., without any refinement via CBM methods), the error in border position compared to histology ground truth was 0.38 ± 0.10 mm for rbCT and 0.81 ± 0.42 mm for fbCT. These strongly positive mean error values showed that the initial border was generally placed significantly outside the true periosteum, and this resulted in average overestimations of a rib's Tt.Ar of 15 ± 3 mm^2 (or 20 ± 3 %) for rbCT, and 30 ± 12 mm^2 (or 39 ± 12 %) for fbCT.

Further comparisons of Ct.Th were made between rbCT and fbCT, albeit without the availability of ground truth histology, using the full rib's surface. Fig. 6 show the average thickness value mapped across the surface of all ribs (whiter regions indicating thicker cortices), with a false-color overlay of the mean thickness differences when analyzing the same physical ribs within rbCT and fbCT scans (green showing regions of bias towards thicker ribs when interpreted via rbCT scans).

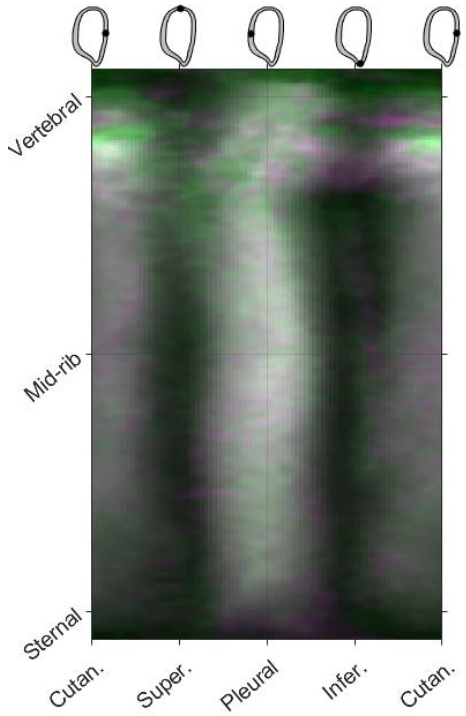

Fig. 6. False-color image of the relative thickness observed using rbCT and fbCT images. Green regions were, on average, identified as being thicker on the isolated rib rbCT images, whereas purple regions were thicker when measured from fbCT images. No clear bias is seen for mid-rib to sternal locations, while vertebral rib end regions are generally seen as thicker when viewed using rbCT images.

IV. DISCUSSION

The goal of this study was to explore how different CT image configurations might affect the quality of the rib bone geometry that can be derived. We have focused on the measurement of local cortical bone thickness, as well as area and inertial properties derived from cross-sectional cuts across a rib's longitudinal axis. Gold standard geometry was obtained via histology images cut across ribs at key locations, and the accuracy and precision of geometry derived using a modified Cortical Bone Mapping technique on CT image volumes was assessed.

Resolution dependence in CBM results

The most consistent difference between the CBM results obtained from fbCT and rbCT was that in all measured quantities the higher resolution rbCT scans produced higher precision. This can be seen in the results listed in Table 2 showing smaller error variance for rbCT scan measurements, as well as in the narrower error distributions for rbCT compared to fbCT as illustrated in Fig. 5. This improvement in precision is to be expected as image resolution increase, and indeed was also reflected within the fbCT scans alone whereby those fbCT scans of highest resolution were marginally more accurate and precise than others. In general, the accuracy (or mean measurement error) was small for both modalities. Of note, there was a slight systematic error in rbCT results that shifted the periosteal border to outside its true position. The precise reason for this is unknown, but may involve the fact that samples were obtained across the same physical distance (from 2mm outside the initial periosteum to 3.5mm inside) in both scans whereas the point spread function inherent in CT imaging tends to produce blur of a physical size related to the image resolution. Another potential source is that the initial surfaces produced via thresholding of each of the two scans can produce significantly different initial periosteal borders (see below for discussion) which the CBM methodology then refines.

Qualitatively, there was little visually discernable difference in Fig. 3 between the overall cortical shells produced by CBM from each scan type and their coherence with ground truth histology. The largest geometric errors were generally attributed to the fbCT scans, and generally found along the superior or inferior rib aspects where the rib cortex was thinnest (see, for example, the 73yo male section in Fig. 3). In these regions, the thin cortex coupled with a large pixel size serves to reduce the CT image intensity well below levels that would generally be considered bone. Here, it is important for an initial segmentation (produced by manual thresholding or other methods) to supply a border to the CBM algorithm that is at least within the vicinity of the true periosteum since the CBM algorithm will only refine borders to within a small (1-2mm) range from the initially provided position.

Potential drawbacks of traditional methods

The results above show that the use of CBM methodology can achieve accuracy and precision in detecting the true position of cortical bone borders that is much smaller than the pixel sizes in the underlying image data. Without such methodology, however, results from the traditional manually-derived rib surface (via thresholding and smoothing) showed a much larger error. The current study predicted that a given rib periosteum built from thresholding of fbCT scans would be placed 0.81 ± 0.42 mm outside of its true location, resulting in 39 ± 12 % overestimation of that rib's total cross-sectional area. Fig. 7 illustrates this overestimation using nearest-neighbor interpolated slices so as to highlight the placement of this initial border around the rbCT and fbCT scan pixels.

Two previous studies have investigated the effect of thresholding CT images of rib cross-sections using images with resolution ranging from 0.4 – 1.0 mm/pixel [6,15]. In these studies, only the direct image pixels of single 2D image slice were used to calculate area, rather than the smoothed periosteal border around those segmented pixels as per the current study. When using a 226 HU threshold, [15] found that rib Tt.Ar was overestimated by 8% and 11% on average for resolutions of 0.4mm/px and 1.0mm/px, respectively, and [6] found that rib Tt.Ar was overestimated by 28% for 2D slices of 0.78mm/px resolution.

To investigate whether the steps performed in this study after thresholding (i.e., the wrapping and smoothing of a 3D surface around segmented pixels) served to artificially inflate the resulting surface beyond the intended transition point of 226 HU, we queried the image intensity of the nearest discrete voxels in 3D space both inside the rib and outside the rib. From within mid-rib cutaneous rib regions (where image intensity reliably reached at

least the 226HU threshold), it was found that 89% of neighbor voxels outside the surface were indeed below the 226HU bone threshold, and 69% of neighbor voxels inside the surface were above that threshold. This indicates that the resulting initial rib surfaces indeed lay along the 226HU transition point, albeit with a slight tendency for that surface to *encompass* voxels of 226HU rather than to pass through their 3D centers.

Overall this has important implications for current HBMs which, in general, have rib geometries that were built using similar thresholding and smoothing techniques to those shown here to overestimate rib cross-sectional size, and from CT images of similar scan resolution. Accurately predicting rib fracture is one of the most difficult tasks of any simulation and it is likely related to most HBMs having unrealistic ribs. This inaccuracy is often in the form of a thick cortex (I.e., cortex location is grossly overpredicted resulting in a "swollen" rib), an evenly distributed cortex (I.e., cortical thickness is the same along the length of the rib or radially around the cortex), and/or a homogenous cortex (I.e., no trabecularization or intracortical porosity [20,21]). It is well established these variables influence experimental rib properties (see [4,6]). Therefore, it is critical that efforts are made to quantify the physical implications of these assumptions on HBM rib behavior and fracture prediction, and if necessary, some foundational alterations made that reflect true rib geometry.

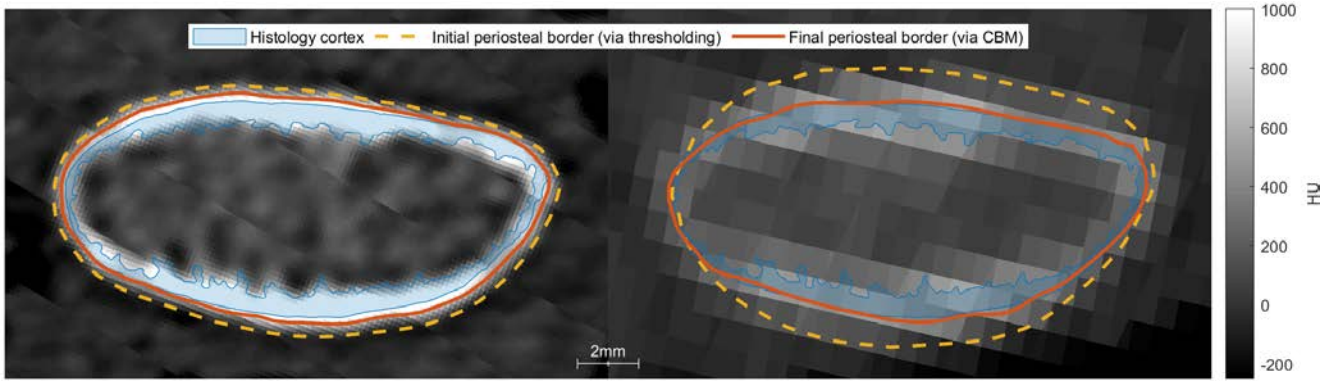

Fig. 7. The error due to partial volume effects when defining the periosteal border for rbCT (left) and fbCT (right) via histogram-based thresholding compared to histology ground truth and the current CBM technique. Errors from simple thresholding are most pronounced in lower resolution scans and can be non-uniformly distributed around the rib.

Study limitations and future work

The current study has focused more on the methodologies used to extract subject rib geometry rather than collecting the breadth of observations from which to quantify typical geometry for a target population. However, the results in this study do suggest that future work should use CBM techniques on targeted populations and in greater subject counts so as to specify the expected rib geometry – as well as its expected variation within the population – in terms of cross-sectional shape and bone thickness. Corridors like this could be directly compared to, and incorporated within, current HBMs so as to better model true rib dynamic behavior.

This study also used only sixth level ribs. The overall morphology of most other rib levels is largely similar to the sixth rib such that they would be expected to perform similarly when interrogated using CBM methods. Only the first rib differs substantially, having a much flatter and wider cross-sectional shape, and it may require a separate specification for its cutaneous and plueral aspects as well as for post-CBM morphological filtering.

The strongest differences in cortical bone thickness between the two scan resolutions in this study (see Fig. 6) occurred near to the vertebral end of the ribs where the undulations in the periosteal surface are present (particularly at the tubercle) and where the rib articulates with the spine. This is due, in part, to the inherent difficulties in separating the *in vivo* ribs from the spine when segmenting fbCT scans, whereas the spine is not present in the isolated rbCT scans. The effects of this difference are seen most clearly at the 10% rib location in Fig. 2, whereby angle differences of the cutting plane due to undulations in the central axis of fbCT scan ribs can produce a cross-section that passes through a marginally different portion of the rib when compared to the rbCT pair. It should be noted that this phenomenon did not affect any histology section sites used for accuracy assessment, the nearest of which was taken at 41% of the rib's length – far from these regions of rapid changes in the rib's surface.

V. CONCLUSIONS

CBM methods yield precise and accurate rib geometry across a variety of CT acquisition parameters, with average errors in the order of -0.04±0.20 mm even for full body scans with a field-of-view covering the whole chest. Consequently, geometric errors (mean and/or SD) in cortical bone cross-sectional area measurements were generally under 13% while errors in total rib cross-sectional area were under 5%. An unacceptably high amount of error is introduced by thresholding techniques without further refinement from CBM, making these traditional techniques unsuitable for analyses wherein rib cross-sectional geometry or bone thickness is important.

VI. ACKNOWLEDGEMENTS

We are grateful for the anatomical donors who made this research possible. Thanks to the faculty, staff, and students of the Injury Biomechanics Research Center, especially Randee Hunter and Victoria Dominguez. Also, Michael Knopp, Karen Briley, and Jim Ellis from the Wright Center of Innovation in Biomedical Imaging, and Brian Ross from the International Center for Automotive Medicine.

VII. REFERENCES

[1] Sirmali, M., Türüt, H., et al. A comprehensive analysis of traumatic rib fractures: morbidity, mortality and management. *European journal of cardio-thoracic surgery*, 2003. 24(1): p. 133-138

[2] Novakov, I., Timonov, P., Stefanov, C., and Petkov, G. Rib fractures in blunt chest trauma-morbidity and mortality: self-experience study. *Trakia Journal of Science*, 2014. 12(3): p. 272-276

[3] Shulzhenko, N.O., Zens, T.J., et al. Number of rib fractures thresholds independently predict worse outcomes in older patients with blunt trauma. *Surgery*, 2017. 161(4): p. 1083-1089

[4] Agnew, A., Murach, M., et al. Sources of Variability in Structural Bending Response of Pediatric and Adult Human Ribs in Dynamic Frontal Impacts. *Stapp car crash journal*, 2018. 62: p. 119-192

[5] Agnew, A., Schafman, M., Moorhouse, K., White, S., and Kang, Y.-S. The effect of age on the structural properties of human ribs. *Journal of the Mechanical Behavior of Biomedical Materials*, 2015. 41: p. 302-314

[6] Murach, M., Kang, Y.-S., et al. Rib Geometry Explains Variation in Dynamic Structural Response: Potential Implications for Frontal Impact Fracture Risk. *Annals of Biomedical Engineering*, 2017: p. 1-15

[7] Kindig, M., Lau, A., and Kent, R. Biomechanical response of ribs under quasistatic frontal loading. *Traffic Injury Prevention*, 2011. 12(4): p. 377-387

[8] Holcombe, S., Wang, S., and Grotberg, J. Modeling female and male rib geometry with logarithmic spirals. *Journal of Biomechanics*, 2016. 49(13): p. 2995-3003

[9] Holcombe, S., Wang, S., and Grotberg, J. The effect of age and demographics on rib shape. *Journal of Anatomy*, 2017. 231(2): p. 229-247

[10] Shi, X., Cao, L., et al. A statistical human rib cage geometry model accounting for variations by age, sex, stature and body mass index. *Journal of Biomechanics*, 2014. 47(10): p. 2277-2285

[11] Wang, Y., Cao, L., et al. A parametric ribcage geometry model accounting for variations among the adult population. *Journal of Biomechanics*, 2016. 49(13): p. 2791-2798

[12] Gayzik, F., Yu, M., Danelson, K., Slice, D., and Stitzel, J. Quantification of age-related shape change of the human rib cage through geometric morphometrics. *Journal of Biomechanics*, 2008. 41(7): p. 1545-1554

[13] Weaver, A., Schoell, S., and Stitzel, J. Morphometric analysis of variation in the ribs with age and sex. *Journal of Anatomy*, 2014. 225(2): p. 246-261

[14] Prevrhal, S., Engelke, K., and Kalender, W.A. Accuracy limits for the determination of cortical width and density: the influence of object size and CT imaging parameters. *Physics in medicine and biology*, 1999. 44(3): p. 751-764

[15] Perz, R., Toczyski, J., and Subit, D. Variation in the human ribs geometrical properties and mechanical response based on X-ray computed tomography images resolution. *Journal of the Mechanical Behavior of Biomedical Materials*, 2015. 41: p. 292-301

[16] Treece, G.M. and Gee, A.H. Independent measurement of femoral cortical thickness and cortical bone density using clinical CT. *Medical Image Analysis*, 2015. 20(1): p. 249-264

[17] Treece, G.M., Gee, A.H., Mayhew, P.M., and Poole, K.E.S. High resolution cortical bone thickness measurement from clinical CT data. *Medical Image Analysis*, 2010. 14(3): p. 276-290
[18] Holcombe, S., Hwang, E., Derstine, B., and Wang, S. Measuring rib cortical bone thickness and cross section from CT. *Medical Image Analysis*, 2018. 49: p. 27-34
[19] Dominguez, V.M. and Agnew, A.M. The use of ROI overlays and a semi-automated method for measuring cortical area in ImageJ for histological analysis. *Am J Phys Anthropol*, 2019. 168(2): p. 378-382
[20] Agnew, A. and Stout, S. Brief communication: Reevaluating osteoporosis in human ribs: The role of intracortical porosity. *American Journal of Physical Anthropology*, 2012. 148(3): p. 462-466
[21] Dominguez, V., Kang, Y., Murach, M., Crowe, N., and Agnew, A. Bone area vs cortical area: Considering intracortical porosity when predicting rib structural properties. *Proceedings of Ircobi Conference*, 2016.